Direct Torque Control for Induction Motor Without Current Sensors

L. Sarah Ancelina
M.E.(Power Electronics & Drives)
PSNA college of engineering & Technology, Dindigul.

I. Gerald Christopher Raj M.E(Ph.d..,)
Associate Professor
PSNA CET

ABSTRACT:

This project presents a low-cost and simple phase-current reconstruction algorithm for three-phase induction motor (IM) under direct torque control (DTC) using the information obtained from only one shunt resistor (in series with low side switches in a conventional three-phase inverter). The aim is to develop a low-cost high-performance IM drive. The proposed algorithm is robust and very simple. It uses the dc current to reconstruct the stator currents needed to estimate the motor flux and the electromagnetic torque. A theoretical concept is developed, the modified look-up table is presented, and current-access tables are designed and used in the phase-current reconstruction. The limitations are also studied and presented. Simulation are given to prove the ability of the proposed scheme of reproducing the performances of a traditional DTC IM drive.

Key words: Direct torque control (DTC), induction motor(IM), sensor count reduction, single current sensor.

I.INTRODUCTION

DIRECT torque control (DTC) of induction motors has gained popularity in industrial applications mainly due to its simple control structure from its first introduction in 1986 [1]. An electric motor drive controlled with the DTC technique exhibits performance similar to a field-oriented drive despite a simpler structure [1], [2]. In fact, a DTC scheme achieves the closed-loop control of the motor stator flux and the electromagnetic torque without using any current loop or shaft sensor.Many researchers are interested in this control technique because of its wide area applications used with various ac machine types as induction motor [3], PMSM [4], [5], PM Brushless [6], and reluctance motor [7]. The DTC scheme requires information about the stator currents and the dc-link voltage, which is used with the inverter switches states, to estimate the values of stator flux and electromagnetic torque. The current feedback for the closed-loop control is usually obtained by sensing instantaneous phase currents by current sensors. In general, galvanically isolated current sensors such as Hall-effect sensors and current transducers are widely used in many applications [8], [9]. Recently, single current sensor operation has been proposed to reconstruct phase currents from the dc-link current sensor [10]. In this way, various approaches have been proposed in the literature. Some methods adjust the pulse-width modulation (PWM) signals to ensure that two-phase currents can be sampled in each control period [11]–[15]. Other strategies introduce modifications of the modulation algorithm in order to guarantee the reliability of the measurements from the dc-link current sensors under all the operating conditions [16]–[18]. Other interesting approaches are based on the estimation of the motor phase currents using prediction-correction algorithms, thus introducing additional computational burden to the drive system [19]–[22]. Only a few papers deal with the DTC technique for induction motor [23] and PMSM [24]. The algorithm used in these works operates in two stages. First, it predicts the stator currents from a model of the motor and then adjusts the prediction on the basis of the sensed dc-link current. This algorithm requires an additional computation burden and the knowledge of the stator transient inductance.In this project, we propose a low-cost single shunt current sensor induction motor (IM) DTC. The stator flux vector and the electromagnetic torque are directly calculated from the voltage and the current derived from a single dc-link voltage sensor (simple voltage divider) and a single dc-link current sensor (simple shunt resistor). The phase currents are estimated by two dc-link current measurement processes. This algorithm does not require additional computation burden or other motor parameter knowledge.

II IDEA OF THE BASIC DTC

The key idea of the basic DTC is slip control, which is based on the fact that, under constant stator flux linkage, the change rate of torque is proportional to the instantaneous slip between the stator flux and rotor . Therefore, torque control can be achieved by means of controlling the slip. There will be eight voltage vectors that can be used for torque and flux control as shown in Figure. It is seen that there are 6 non-zero vectors and 2 zero vectors.

Under the basic DTC, the flux and torque control are carried out by means of a switching table, as shown in Figure2.1 the flux plane is divided into 6 sectors. In each sector, there are four non-zero vectors and two zero vectors that are needed to control the flux and torque. Each vector has different effect on the torque and flux linkage. For example, if the flux linkage vector is in sector 1, voltage vector V3 (011) used to increase both the torque and the flux linkage. V4 (100) is used to decrease the both. V2 (010) is used to increase torque

and reduce the amplitude the flux linkage. V5 (101) is used to reduce the both.

If the voltage drop on the stator resistance is neglected, it can be assumed that the flux linkage is always following the direction of the voltage vector. And for each vector, there are two components, one for controlling torque and the other one flux linkage. It is seen that the torque and the flux component are different at different position. It should also be noted that in each border of the 6 sectors, the ability of controlling the flux linkage is very weak sometime, as reported in .

Therefore, if more vectors are used in one sampling interval, maybe a better performance can be expected. And that is the basis of the modified DTC. Under the modified scheme, 3 vectors are used to control flux, such that the amplitude of flux and torque can be controlled.

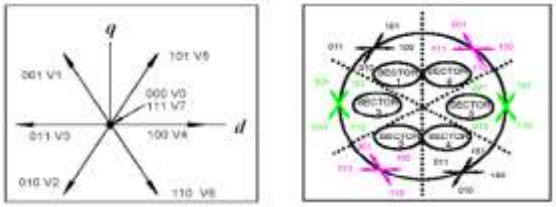

Figure 2.1Eight voltage space vectors generated by a 3φ 2 level inverter

III SELECTION TABLE FOR DTC

The equation for the developed torque of an induction motor may be expressed in terms of the stator and rotor flux space vector as in equation (3.I)

$$T = \frac{X_m}{X_s X_r - X_m^2} |\psi_s| |\psi_r| \sin \delta_\psi \qquad (3.1)$$

where δ_Ψ, denotes the angle between the stator and the rotor flux space vectors, X_s, X_r, and X_m, represent the stator, rotor and airgap self inductions, respectively. For a constant magnitude of the stator and rotor flux space vectors, the angle δ_Ψ may be used to control the torque of the motor. The following expression may be obtained from the stator voltage equation of the induction motor model

$$\psi_s = \frac{1}{T_n} \int_0^t V_s dt \qquad (3.2)$$

where T_n, denotes the electrical time constant and V_s, the stator voltage space vector. This expression is valid for a stator fixed reference frame and a stator resistance equal to zero. It can be seen that the stator voltage directly impresses the stator flux. The stator voltage space vector V_s, may assume six different non zero states and two zero states as shown in Figure 3.1

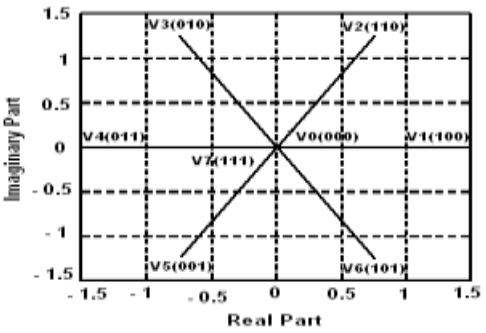

Figure 3.1 voltage vectors of 3φ PWM inverter

The change of the stator flux vector per switching instant is therefore determined by equation (3.2) and Figure 3.1. The change of the magnitude of stator flux space vector and the change of the torque with varying angle of the stator flux space vector are shown in Figure 3.2, respectively. It may be seen from the figures that the change of stator flux and torque is sinusoidally distributed over the stator flux angle for the non zero voltage vectors V1 to V6 and is constant for the zero vectors V0, and V7. The dc offset of all sinusoids coincides with the line for voltage vectors V0 and V7.

For example it may be seen, that the application of voltage vector V2, in the centre of section S2 (60 degrees) causes the maximum stator flux increase possible for a given time interval and a given dc link voltage. However, it also causes the developed torque to decrease as shown in Figure 3.2. It has been obtained that the amplitudes, phase shifts and dc levels for the sinusoids in Figure 3.2do not vary with different motor speed and load torque conditions.

The phase shift of the motor torque changes increases only marginally (approx. 5 degrees) for high speed, high load torque operation. However, the dc offset of the sinusoids in Figure 3.2 changes considerably with motor condition. The zero change line tends to move upwards when the motor speed is increased. Therefore, less positive torque change may be obtained and thus the maximum motor speed is limited.

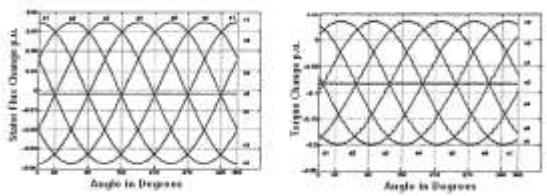

Figure 3.2 Flux and Torque change in 100μs

Smilarly, for low speed operation, the zero change line moves towards the negative peaks in Figure 3.4, thus positive torque changes are easily obtained. Since the sequence of the stator flux and torque changes for the voltage vectors V0 to V7 remains unchanged, a selection table as shown in Table 3.1 may be obtained to control the stator flux and torque of an induction motor.
The sections of the stator flux space vector are denoted as S1 to S6, according to Figure 3.2. The magnitude error of the stator flux space vector is denoted by Φ. If Φ = 1 then the stator flux level is too low and therefore the voltage vectors V2 or V6 are selected, which cause a positive flux change, as can be seen from Figure 3.2.

b_Φ	b_Γ	Sector I	Sect II	SectI II	Sect IV	Sect V	Sect VI
1	1	V_5	V_6	V_1	V_2	V_3	V_4
	0	V_3	V_4	V_5	V_6	V_1	V_2
0	1	V_6	V_1	V_2	V_3	V_4	V_5
	0	V_2	V_3	V_4	V_5	V_6	V_1

Table 3.1 selection table for DTC

The torque error is represented by T and T = -1 denotes that the developed torque is too high and can be decreased by selecting V6 if the angle of the stator flux vector is in section S1 (Table 3.1 and Figure 3.2). Similarly, the torque can be increased by selecting V2 for T = 1. The zero voltage vectors V0 and V7 are selected when the torque error is within the given hysteresis limits.

IV SINGLE CURRENT SENSOR DTC SCHEME

The basic DTC scheme (see Fig. 1) requires two current sensors at least. The proposed DTC scheme described in this paper uses only one shunt resistor for dc-link current measurement as revealed on Fig. 3. For this purpose, a suitable method to reconstruct the phase currents and voltages is devised with a simple modification of the basic DTC scheme using zone shift strategy. Two modifications of the basic DTC are used for estimating the three-phase currents from a single dc-link current sensor. On the first modification, the control system should be able to generate more voltage vectors. This goal can be

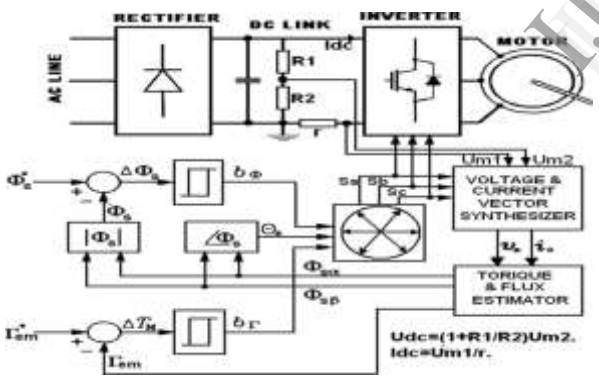

Fig. 4.1 Proposed DTC scheme.

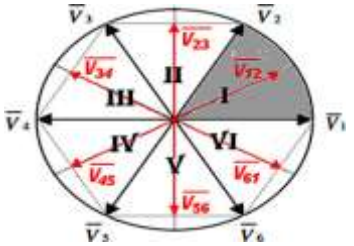

Fig. 4.2 Proposed DTC sectors and inverter voltage vectors.

approximately by applying, at each cycle period, different voltage vectors for prefixed time intervals, leading to a discrete SVM technique. By using this modulation strategy, new voltage vectors can be synthesized with respect to those used in the basic DTC technique. It has been verified that subdividing the cycle period in two equal time intervals leads to a substantial reduction of current sensors without the need for too complex switching tables. Using the DSVM technique with two equal time intervals, 12 new voltage vectors can be generated; we use only six active voltage vectors in our proposed DTC scheme as represented in Fig. 4.1. The red vectors represent the synthesized voltage vectors.

As the zone shift strategy, one other modification results in improving the DTC by using a new lookup table and adjusting the six stator flux sectors of the conventional DTC (see Fig. 2). The first sector is taken from 0◦ to 60◦ (see Fig. 4.2), instead of −30◦ to 30◦. The new operation table of the modified DTC is presented in Table II.

b_Φ	b_Γ	Sect I	Sect II	Sect III	Sect IV	Sect V	Sect VI
1	1	V_{56}	V_{61}	V_{12}	V_{23}	V_{34}	V_{45}
	0	V_{34}	V_{45}	V_{56}	V_{61}	V_{12}	V_{23}
0	1	V_{61}	V_{12}	V_{23}	V_{34}	V_{45}	V_{56}
	0	V_{23}	V_{34}	V_{45}	V_{56}	V_{61}	V_{12}

TABLE II
PROPOSED DTC SWITCHING TABLE

V DC-LINK CURRENT SAMPLING ANDSTATORCURRENT RECONSTRUCTION

One of the most important purposes for single-shunt threephase reconstruction is to reduce the cost. This, in turn, simplifies the sampling circuit to one shunt resistor and some other electronic components. Moreover, the single-shunt algorithm allows the use of power modules that do not provide, for each phase, individual ground connection. Another single-shunt measurement advantage is that the same circuit is being used to sense all three phases. For all measurements, the gains and offset will be the same, which eliminate the software calibration of each phase measurement structure.

Sampling Time

Both dc-link current sampling instants must be chosen for the application of the three-phase-current reconstruction concept. In accordance with Fig. 5

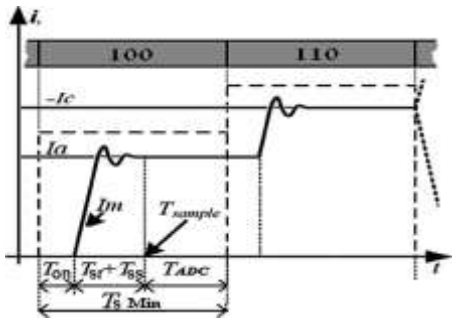

Fig. 5 Recurred sampling time.

the optimal sampling instants should be calculated relatively to the active vector transition instants. For a consistent dc-link current value, the signal sampling must take place after an additional delay

*T*sample ≥ *T*on + *T*sr + *T*ss . (9)The sample time includes the total switching device turn-on delay time *T*on), the dc-link current signal rise time (*T*sr), and the signal settling time (*T*ss). The *T*on parameter includes the dead-time, the insulated gate bipolar transistor (IGBT) driver signal processing time, and the worst case switching device (IGBT) on-time delay. The parameter *T*ss is related to the signal amplifiers and the isolation circuit. Once the sampling is started, the process requires an extra sample-and-hold time delay (*T*ADC). The latter can be important, particularly in the case of a low-cost DSC ADC. However, all these delays may be neglected compared to the DTC control period. The sampling instant chosen in the proposed phase current reconstruction is at the end of each half period when the dc current signal is stabilized.

The smallest DTC control period is given by *T*s ≥ 2 (*T*on + *T*sr + *T*ss + *T*ADC) (10) Actually, the sum of all these time delays is about a few microseconds, even with the isolation system, which is far smaller compared to 50 μs used in our system. Fig. 5.1

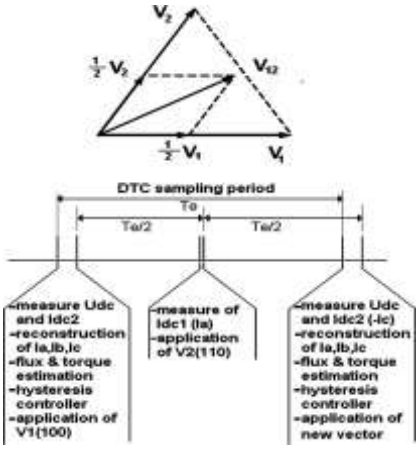

illustrates the example of recurred sampling time when the voltage vector $V_{12}$is applied.

VI. Inverse Sine PWM

The control strategy uses the same reference (synchronized sinusoidal signal) as the conventional SPWM while the carrier triangle is a modified one. The control scheme uses an inverted (high frequency) sine carrier that helps to maximize the output voltage for a given modulation index. Enhanced fundamental component demands greater pulse area. The difference in pulse widths (hence area) resulting from triangle wave and inverted sine wave with the low (output) frequency reference sine wave in different sections can be easily understood. In the gating pulse generation of the proposed ISCPWM scheme shown in Fig. 6.1

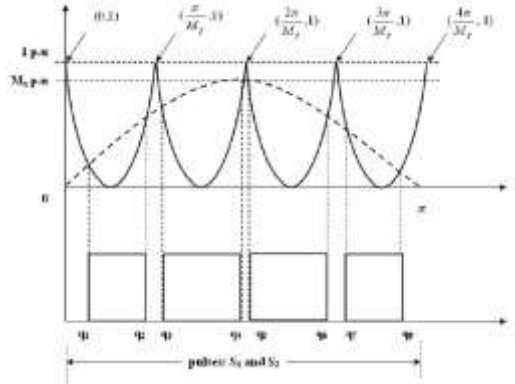

Fig. 6.1 Inverter sine carrier PWM pulse pattern.

the triangular carrier waveform of SPWM is replaced by an inverter sine waveform. For the ISPWM pulse pattern, the switching angles may be computed as the same way as SPWM scheme. It is worthwhile to note that both in SPWM (considered) and ISCPWM schemes, the number of pulses will be equal to f M and hence the constant
switching loss is guaranteed. To have conceptual understanding of wider pulse area and hence the dexterous input dc utilization in the ISCPWM, location of switching angles, duty cycle and their dependence on a M and f M are discussed. Fig. 6.2depicts the influence of a M on different switching angles (four angles considered in both cases) at constant f M of 6. From this figure, it is observed that the odd switching instants vary with negative slope and even Inverted Sine Carrier for switching instants have positive slope. Variation of all the switching instants against a M is a straight line and slope of each one is more than its previous one. All the odd switching angles of ISCPWM method happen earlier than similar angles of PWM method, while the situation is reverse in case of even switching angles and hence higher pulse area. Both SPWM and ISCPWM upshots nonlinear relationship in the lower f M range.

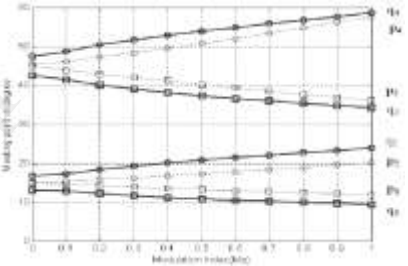

Fig. 6.2 – Influence of modulation index on switching angles.

VII.SIMULATION RESULTS

A simulation model is established to MATLAB/SIMULINK model-based on power system toolbox was developed to examine the proposed control algorithm and the phase-current reconstructionfeasibility.

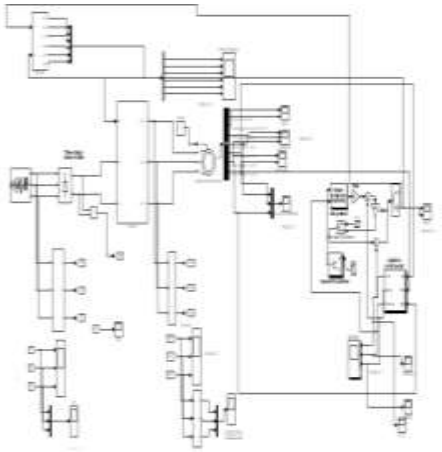

Figure 7.Simulation diagram

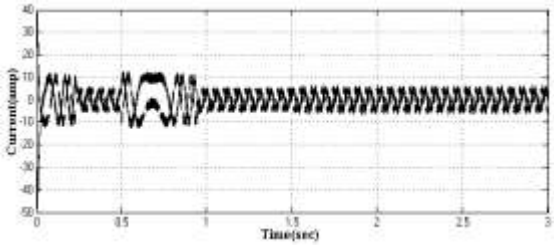

Figure 7.1 Current Waveform of Basic DTC

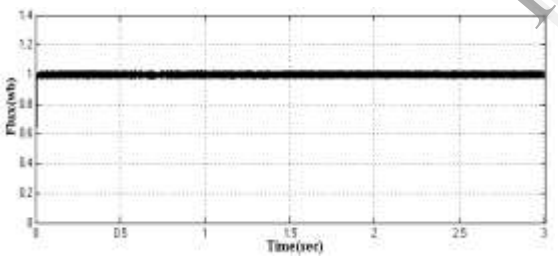

Figure 7.2 Flux Waveform of Basic DTC

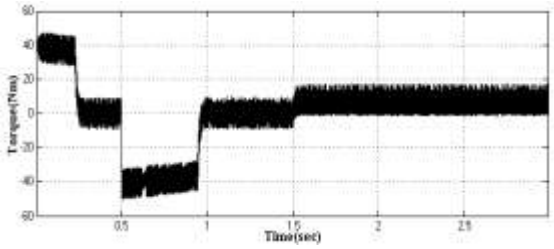

Figure 7.3 Torque Waveform of Basic DTC

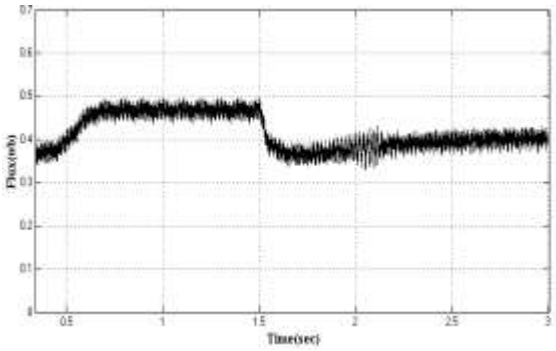

FIGURE 7.4 FLUX WAVEFORM OF MODIFIED DTC

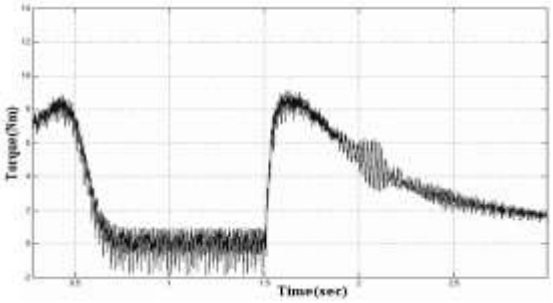

Figure 7.5 Torque Waveform of Modified DTC

VII.CONCLUSION

This project presents a new direct torque and flux control strategy based on two pi controllers and a voltage space-vector modulator. the main conclusions are as follows.

• DTC-ISPWM strategy realizes almost ripple-free operation for the entire speed range. Consequently, the flux, torque, and speed estimation is improved.

• The fast response and robustness merits of the basic DTC are entirely preserved.

• The switching frequency is constant and controllable. in fact, the better results are due to the increasing of the switching frequency. While for DTC a single voltage vector is applied during one sampling time, for DTC-ISPWM a sequence of six vectors is applied during the same time. It can be stated that, using the DTC-ISPWM topology, the overall system performance is increased

VIII.REFERRENCES

[1] I. Takahashi and T. Noguchi, "A new quick-response and high-efficiency control strategy of an induction motor," *IEEE Trans. Ind. Appl.*, vol. IA- 22, no. 5, pp. 820–827, Sep./Oct. 1986.

[2] S. A. Zaid, O. A. Mahgoub, and K. El-Metwally, "Implementation of a new fast direct torque control algorithm for induction motor drives," *IETE lectr. Power Appl.*, vol. 4, no. 5, pp. 305–313, May 2010.

[3] C. Patel, R. P. P. A. Day, A. Dey, R. Ramchand, K. K. Gopakumar, and M. P. Kazmierkowski, "Fast direct torque control of an open-end induction motor drive using 12-sided polygonal voltage space vectors," *IEEE Trans. Power Electron.*, vol. 27, no. 1, pp. 400–410, Jan. 2012.

[4] Y. Zhang and J. Zhu, "Direct torque control of permanent magnet synchronous motor with reduced torque ripple and commutation frequency," *IEEE Trans. Power Electron.*, vol. 26, no. 1, pp. 235–248, Jan. 2011

[5] Y. Zhang and J. Zhu, "A novel duty cycle control strategy to reduce both torque and flux ripples for DTC of permanent magnet synchronous motor drives with switching frequency reduction," *IEEE Trans. Power Electron.*, vol. 26, no. 10, pp. 3055–3067, Oct. 2011.

[6] K. D. Hoang, Z. Q. Zhu, andM. P. Foster, "Influence and compensation of inverter voltage drop in direct torque-controlled four-switch three phase PM brushless AC drives," *IEEE Trans. Power Electron.*, vol. 26, no. 8, pp. 2343–2357, Aug. 2011.

[7] S. Bolognani, L. Peretti, and M. Zigliotto, "Online MTPA control strategy for DTC synchronous-reluctance-motor drives," *IEEE Trans. Power Electron.*, vol. 26, no. 1, pp. 20–28, Jan. 2011.

[8] G. Foo and M. F. Rahman, "Direct torque and flux control of an IPM synchronous motor drive using a backstepping approach," *IET Elect.Power Appl.*, vol. 3, no. 5, pp. 413–421, Sep. 2009.

[9] M. E. Haque and M. F. Rahman, "Incorporating control trajectorieswith the direct torque control scheme of interior permanent magnet synchronous motor drive," *IET Elect. Power Appl.*, vol. 3, no. 2, pp. 93–101 Mar. 2009.

[10] T. C. Green and B. W. Williams, "Derivation of motor line-current waveforms from the dc-link current of an inverter," in *Proc. IEE Elect. Power Appl.*, Jul. 1989, vol. 136, no. 4, pt. B, pp. 196–204.

[11] W. C. Lee,T. K. Lee, andD. S.Hyun, "Comparison of single-sensor current control in the dc link for three-phase voltage-source PWM converters," *IEEE Trans. Ind. Electron.*, vol. 48, no. 3, pp. 491–505, Jun. 2001.

[12] J. T. Boys, "Novel current sensor for PWM AC drives," in *Proc Electr. Power Appl.*, 1988, vol. 135, pt. B, pp. 27–32.